SPATIAL INTERMITTENCY IN TWO-DIMENSIONAL TURBULENCE: A WAVELET APPROACH

KAI SCHNEIDER
L3M–CNRS & CMI, Université de Provence, Marseille, France
Email: kschneid@cmi.univ-mrs.fr

MARIE FARGE
LMD–IPSL–CNRS, École Normale Supérieure, Paris, France
Email: farge@lmd.ens.fr

NICHOLAS KEVLAHAN
Department of Mathematics and Statistics, McMaster University, Hamilton, Canada
Email: kevlahan@mcmaster.ca

Turbulence is characterized by its intermittency, which is defined classically as localized bursts of small-scale activity in the observed quantity (*e.g.* velocity, vorticity, dissipation). Consequently, the simultaneous space and scale localization of the wavelet representation makes it a natural choice for studying intermittency. We propose different measures of intermittency, based on orthogonal wavelets, which avoid some problems associated with classical measures. We then apply them to study the intermittency of two-dimensional turbulence computed by direct numerical simulation.

1 Introduction

Turbulence is considered fully-developed when nonlinear effects, due to the advection terms of the Navier–Stokes equation, strongly dominate linear effects due to the dissipative terms. Intermittency, namely isolated bursts of activity in the measured quantity, has long been recognized as an essential characteristic of fully-developed turbulent flows. When introducing the energy spectrum as the Fourier transform of the two-point correlation Taylor [33], noted that dissipation is distributed unevenly:

> ...the fact that small quantities of very high frequency disturbances appear, and increase as the speed increases, seems to confirm the view frequently put forward by the author that the dissipation of energy is due chiefly to the formation of very small regions where the vorticity is very high. Apart from these very small regions the turbulence behind a grid is similar at all speeds.

Taylor already had the intuition that bursts of high frequency vorticity are responsible for dissipation. This is what we now refer to as spatial intermittency.

Soon afterwards Kolmogorov [17] and Obukhov [26] introduced their theory of homogeneous isotropic turbulence, where energy is transferred inviscidly in the inertial range from large to small scales until it is finally dissipated at the smallest scales of motion. In their theory Kolmogorov and Obukhov assumed that the dissipation of energy is space-filling (*i.e.* non-intermittent). However, in 1944 Landau noticed that the spectral energy transfer rate cannot be constant in space, and thus

the fluctuation of energy dissipation must be intermittent at small scales. This is consistent with the physical intuition of Taylor [33]. To correct his original theory for intermittent dissipation, Kolmogorov [18] supposed that the dissipation at small scales is distributed log-normally in space. This correction leads to a small increase in the slope of the energy spectrum in the inertial range.

The first quantitative estimation of intermittency was presented by Townsend [34]. He pictured turbulence as a sequence of active bursts separated by quiescent regions. To quantify this intermittency he introduced an 'intermittency factor' γ which measures the ratio of active regions to quiescent regions ($\gamma = 1$ corresponds to an entirely active signal, $\gamma = 0$ corresponds to an entirely quiescent signal). He showed that γ is inverse proportional to flatness

$$F = \frac{\langle f^4 \rangle}{\langle f^2 \rangle^2} = \frac{3}{\gamma}, \tag{1}$$

where f is the signal and $\langle \cdot \rangle$ denotes the average. The flatness is now one of the standard measures of intermittency. Batchelor & Townsend [2] used this tool to study the intermittency of the first three derivatives of the velocity, finding that flatness increases with the order of derivatives for isotropic turbulence as well as for the wake behind a cylinder. This increase in flatness was attributed to the presence of coherent vortices produced by nonlinear instabilities.

Because intermittency is associated with the small scales, many studies involved signal filtering to extract either the small scales, or a range of scales. This filtering is done in Fourier space, and the filtered signal is transformed back to physical space before computing its flatness using (1). Sandborn [29] employed a constant relative band-width filter to measure flatness of the longitudinal velocity fluctuations as a function of wavenumber in channel flow boundary layers. He found that the flatness increases strongly with wavenumber, *i.e.* the smaller the scale the more intermittent the flow, independently of the distance from the wall. Note that the constant relative band-width filter ($\Delta k/k$ constant) used by Sandborn has the same spectral properties as the wavelet filters we consider later.

It is important at this point to mention that, although these experiments attempt to study spatial intermittency, they use time series data (from a fixed probe in a mean flow) which are interpreted in terms of spatial series using Taylor's hypothesis [33]

$$\frac{\partial}{\partial x} = -\frac{1}{U}\frac{\partial}{\partial t}, \tag{2}$$

where the mean velocity U is supposed to be much larger than the fluctuation velocity. Note that this hypothesis is valid only on average. However, some intense turbulent fluctuations may exceed U, which would then cause Taylor's hypothesis to fail. In addition, Lin [20] showed that Taylor's hypothesis is not strictly valid for flows with mean gradients (*e.g.* shear flows, boundary layers). Thus, experimental measurements of intermittency may not always be reliable estimates of spatial intermittency. In the case of numerical simulations (as analyzed below), Taylor's hypothesis is not required to study spatial intermittency.

Following the method proposed by Sandborn [29], Kennedy & Corrsin [16] used a band-pass filter with constant relative bandwidth to study intermittency in a

free jet. They compared the flatness of the turbulent velocity fluctuations with the flatness of a squared Gaussian process as a function of scale, in order to see whether nonlinear processes might be responsible for turbulence intermittency. They found that squared Gaussian noise is more intermittent at all scales than the turbulent fluctuations, although flatness increases with decreasing scale in both cases. They also remarked that averaging tends to make a non-Gaussian signal appear Gaussian (*i.e.* flatness converges to 3).

The intermittent character of turbulence affects other diagnostics used for its study:

- the slope of the inertial range energy spectrum is steepened,
- the exponent ζ_p of the $p-$th order structure function,

$$\langle |u(x+l) - u(x)|^p \rangle \propto l^{\zeta_p}, \tag{3}$$

  increases more slowly than linearly with p,
- ratios of subsequent moments grow with the order of the moments, *i.e.* $M_4/M_2^2 < M_6/M_3^2 < \ldots$, where the moment of order p is defined as $M_p = \langle u^p \rangle$. This implies that the probability density function (PDF) decays slower than a Gaussian at large values (this characteristic is often called 'heavy tails'),
- as suggested by Batchelor & Townsend [2] and others, intermittency is linked to the presence of coherent vortices in the flow.

Hence, any physically sound model of turbulence must take into account intermittency. Currently, the most physically accurate turbulence model is large eddy simulation (LES), but it takes into account only a weak intermittency limited to the resolved scales of the flow, namely the large eddies. Let us mention here that from our point of view large eddies are not the same as coherent vortices. We have shown previously [12,10,9] that coherent vortices, *i.e.* localized concentrations of energy and enstrophy which survive on times much longer than the eddy turn-over time, are multiscale structures. Consequently, the low-pass filters used in LES remove the small-scale part of coherent vortices.

The goal of this paper is to point out the limitations of classical measures of intermittency, and to present a unified set of wavelet-based alternatives (many of which have been introduced separately elsewhere). We show how the classical measures can be thought of as a special case of wavelet filtering using a singular wavelet. It is this lack of regularity that limits the usefulness of classical measures for sufficiently smooth signals.

In the following section we review classical methods for studying intermittency and note their drawbacks which lead to incorrect results in certain cases. In §3 we present wavelet-based methods that overcome these limitations, and produce accurate results in all cases. We also show precisely how the wavelet methods relate to the classical methods reviewed in §2. The differences between the two approaches are then illustrated by applying them to a direct numerical simulation (DNS) of two-dimensional turbulence in §4. In particular, we see that, in this cas, the classical structure function gives the wrong result when applied to the velocity

field, whereas the appropriate wavelet equivalent works correctly. Finally, in §5 we summarize the main results of this paper.

2 Classical methods for studying intermittency

As we noted in the introduction, intermittency is defined as localized bursts of high frequency activity. This means that intermittency is a phenomenon localized in both physical space and spectral space, and thus a suitable basis for representing intermittency should reflect this dual localization. The Fourier basis is perfectly localized in spectral space, but fully delocalized in physical space. Therefore when a turbulence signal is filtered using a high-pass Fourier filter and then reconstructed in physical space, *e.g.* to calculate its flatness, some spatial information is lost. This leads to smoothing of strong gradients and the appearance of spurious oscillations in the background, which come from the fact that the modulus and phase of the discarded high wavenumber Fourier modes have been lost. The spatial errors introduced by such a filtering lead to errors in estimating the flatness, and hence intermittency, of the signal.

When a quantity (*e.g.* velocity derivative) is intermittent it contains rare but strong events (*i.e.* bursts of intense activity), which correspond to large deviations reflected in the 'heavy tails' of the PDF. Second-order statistics (*e.g.* energy spectrum, second-order structure function) are relatively insensitive to such rare events because their time or space support is very small and thus do not dominate the integral. However, these events become increasingly important for higher-order statistics, and finally come to dominate. High-order statistics therefore characterize intermittency. Of course, intermittency is not essential for all problems: second-order statistics will suffice to measure dispersion (dominated by energy-containing scales), but not to calculate drag (dominated by vorticity production in thin boundary layers).

Classical examples of high-order statistics are the pth-order structure functions. In §3.5 we will see that structure functions correspond to the L^p-norm of the wavelet coefficients using the wavelet difference of Diracs (DOD) wavelet [4], which has only a single zero moment (the minimum required for a wavelet). We will show that this limits the usefulness of the structure functions for analyzing sufficiently smooth fields. The drawback of higher-order statistics, however, is that the number of samples required for an accurate estimation increases with order p. For instance, the number of samples required to estimate the moments of order 12 is about 10^9, and thus estimation of high-order moments quickly becomes impractical.

To circumvent this difficulty we have proposed a different approach: namely to separate the rare and extreme events from the dense and weak events, and then calculate the statistics for each independently. In turbulent flows the rare events are the coherent vortices and the dense events correspond to the incoherent background flow. A major difficulty in turbulence theory is that there is no clear scale separation between these two kinds of events. This lack of a 'spectral gap' excludes Fourier filtering. Since the rare events are well localized in physical space one might try using an on-off filter in physical space to extract them, but in this case you need an *a priori* model of the coherent structures. However, this approach changes the

spectral properties by introducing spurious discontinuities (adding an artificial k^{-2} component to the energy spectrum). To avoid these two problems we propose using the wavelet representation, which combines both physical and spectral localization (bounded from below by Heisenberg's uncertainty principle). We have shown [10] that nonlinear wavelet filtering can be used to separate the coherent vortices from the background flow. Since we have extensively discussed the use of wavelets for conditional averaging in previous work (*e.g.* [10]), in this paper we focus on the use of wavelets in the context of L^p-norms.

The most basic L^p-norms are the pth-order moments. They are defined for a quantity f with PDF $P(f)$ as

$$M_p(f) = \int P(f) f^p df. \tag{4}$$

One can then calculate the ratios of moments of different orders

$$Q_{p,q}(f) = \frac{M_p(f)}{(M_q(f))^{p/q}}. \tag{5}$$

The $Q_{p,q}(f)$ measure the shape of the distribution $P(f)$. For example, if $q = 2$ we can define the following quantities:

- skewness $S = Q_{3,2}(f)$,
- flatness $F = Q_{4,2}(f)$,
- hyperskewness $S_h = Q_{5,2}(f)$,
- hyperflatness $F_h = Q_{6,2}(f)$.

The departure of the PDF from Gaussianity can then be measured by comparing the above quantities to their values in the Gaussian case (*e.g.* $S = 0, F = 3$ for a Gaussian distribution).

The p–th order structure function is used extensively to study homogeneous turbulence since it is translation invariant, characterizes the self-similar structure of the flow and is easy to measure experimentally. The p–th order structure function of a random scalar field f is defined as

$$S_{p,f}(l) \;=\; \langle |f(x+l) - f(x)|^p \rangle \;. \tag{6}$$

Note that under assumptions of self-similarity and using the (exact) Karman-Howarth expression for the third-order structure function $S_p(l) \sim l^{p/3}$, *i.e.* a straight line on a log-log graph. However, experimental measurements fall below this straight line prediction.

A related second-order statistic is the spectrum

$$E(k) = \frac{1}{2}|\hat{f}(k)|^2 \qquad \text{with} \quad \hat{f}(k) = \frac{1}{2\pi}\int f(x)\exp(-ikx)dx \quad , \tag{7}$$

which is related to the second-order structure function $S_{2,f}(l)$ and the autocorrelation function $R(l)$ in the following way,

$$R(l) = \; \langle f(x+l)f(x) \rangle \;=\; 2\int_0^\infty \cos(kl)E(k)dk, \tag{8}$$

and hence we get

$$S_{2,f}(l) = \langle |f(x+l) - f(x)|^2 \rangle = 2R(0) - 2R(l) \tag{9}$$

$$= 2\int_0^\infty (1 - \cos(kl))E(k)dk. \tag{10}$$

The above relation shows that the structure function corresponds to a filtered spectrum, and the corresponding filter is insensitive to sufficiently smooth fields. In §3.5 we will propose wavelet tools to improve the filter selectivity.

3 Wavelet methods for studying intermittency

3.1 Orthogonal wavelet transform

In this section we describe some statistical tools based on the orthogonal wavelet transform. The wavelet approach avoids the limitations of structure functions and allows moment ratios to be defined as a function of scale. We present them considering, as example, a one-dimensional scalar field $f(x)$ which has vanishing mean and is periodic (the extension to higher dimensions and vector fields is straightforward). Hence we employ a periodic multi-resolution analysis (MRA) [6,11,23] and develop the signal f, sampled on $N = 2^J$ points, as an orthonormal wavelet series from the largest scale $l_{max} = 2^0$ to the smallest scale $l_{min} = 2^{-J}$:

$$f(x) = \sum_{j=0}^{J-1} \sum_{i=0}^{2^j-1} \tilde{f}_{j,i}\, \psi_{j,i}(x), \tag{11}$$

where $\psi_{j,i}$ is the 2π-periodic wavelet. Due to orthogonality the coefficients are given by $\tilde{f}_{j,i} = \langle f, \psi_{j,i} \rangle$ where $\langle \cdot, \cdot \rangle$ denotes the L^2-inner product. The wavelet coefficients are indexed in terms of scale j, position i.

3.2 Wavelet spectra

We define the scale distribution of energy, also called scalogram, as

$$E_j = \sum_{i=0}^{2^j-1} |\tilde{f}_{j,i}|^2. \tag{12}$$

To be able to relate the scale distribution to the Fourier spectrum, we introduce the mean wavenumber k_0 of the wavelet ψ, defined by

$$k_0 = \frac{\int_0^\infty k|\widehat{\psi}(k)|dk}{\int_0^\infty |\widehat{\psi}(k)|dk}. \tag{13}$$

Thus each scale 2^{-j} of the wavelet ψ_j is inversely proportional to the mean wavenumber $k_j = k_0 2^j$. The discrete local wavelet spectrum [8,28] is then defined as

$$\widetilde{E}(k_j, x_i) = |\tilde{f}_{j,i}|^2 \frac{2^j}{\Delta k_j}, \tag{14}$$

where $\Delta k_j = \sqrt{k_j k_{j+1}} - \sqrt{k_j k_{j-1}}$ is the mean wavenumber.

By measuring $\widetilde{E}(k_j, x_i)$ at different positions x_i in a turbulent flow one can study how the energy spectrum depends on local flow conditions, and estimate the contribution to the overall Fourier energy spectrum of different components of the flow. For example, one can determine the scaling of the energy spectrum contributed by coherent structures, such as isolated vortices, and the scaling of the energy spectrum contributed by the incoherent background flow.

The spatial variability of the local energy spectrum $\widetilde{E}(k_j, x_i)$ measures the flow's intermittency. This quantity also allows us to study the global spectral behaviour of f by summing the local energy spectrum over all positions,

$$\widetilde{E}(k_j) = \sum_{i=0}^{2^j-1} \widetilde{E}(k_j, x_i). \tag{15}$$

The relationship between the global wavelet spectrum $\widetilde{E}(k_j)$ and the usual Fourier energy spectrum $E(k)$ is described in the following section.

3.3 Relation between wavelet and Fourier spectra

First note that due to the orthogonality of the wavelet decomposition, the total energy is preserved and we have $E = \sum_j E_j$. The global wavelet spectrum is related to the Fourier energy spectrum according to [28,11]

$$\widetilde{E}(k) = \frac{1}{C_\psi k} \int_0^\infty E(k') |\widehat{\psi}(k_0 k'/k)|^2 dk'. \tag{16}$$

where

$$C_\psi = \int_0^\infty \frac{|\widehat{\psi}(k)|^2}{k}\, dk. \tag{17}$$

The wavelet spectrum is therefore a smoothed Fourier spectrum weighted by the modulus of the Fourier transform of the analyzing wavelet [28]. Note that, as the wavenumber increases, the smoothing interval becomes larger [11]. A sufficient condition guaranteeing that the global wavelet spectrum is able to detect the same power-law behaviour $k^{-\alpha}$ as the Fourier spectrum is that ψ should have enough vanishing moments m [28], *i.e.*

$$\int_{-\infty}^{+\infty} x^m \psi(x)\, dx = 0 \quad \text{for} \quad 0 \le m \le \frac{\alpha - 1}{2}. \tag{18}$$

If this condition is not satisfied the global wavelet spectrum saturates at the critical cancellation order m. In this case it only shows a power-law behaviour with a slope not steeper than $\alpha = 2(m + 1)$. Since large α corresponds to smooth functions, when the analyzed function is smoother than the wavelet, then $\psi(x)$ should have more vanishing moments m in order to correctly detect the slope of the signal's spectrum. If the wavelet does not have enough zero moments we simply measure the spectral scaling of the wavelet and not of the signal!

3.4 Wavelet intermittency measures

In this section we use the space-scale information contained in the wavelet coefficients to define scale-dependent moments and moment ratios. Useful diagnostics to quantify the intermittency of a field are the moments of its wavelet coefficients at different scales j [30],

$$M_{p,j}(f) = \frac{1}{2^j} \sum_{i=0}^{2^j-1} |\tilde{f}_{j,i}|^p. \tag{19}$$

Note that (12) implies $E_j = 2^j M_{2,j}$.

The sparsity of the wavelet coefficients at each scale is a measure of intermittency, and it can be quantified using ratios of moments at different scales,

$$Q_{p,q,j}(f) = \frac{M_{p,j}(f)}{(M_{q,j}(f))^{p/q}} \quad , \tag{20}$$

which may be interpreted as quotient norms between different L^p- and L^q-spaces. Classically, one chooses $q = 2$ to define typical statistical quantities as a function of scale. Recall that for $p = 4$ we obtain the scale dependent flatness $F_j = Q_{4,2,j}$, which is equal to 3 at all scales j for a Gaussian white noise (non intermittent signal). The scale dependent skewness, hyperflatness and hyperskewness are obtained for $p = 3, 5$ and 6, respectively. For intermittent signals $Q_{p,q,j}$ increases with j.

3.5 Relation to structure functions

In this section we link the scale dependent moments of wavelet coefficients with structure functions. In the case of second order statistics, we show that global wavelet spectra correspond to second order structure functions. Furthermore, we give a rigorous bound for the maximum exponent of the structure functions and propose a way to overcome this limitation.

The increments of a signal, also called the modulus of continuity, can be seen as its wavelet coefficients using the DOD wavelet mentioned earlier, *i.e.*

$$\psi(x) = \delta(x+1) - \delta(x). \tag{21}$$

We thus obtain

$$u(x+l) - u(x) = \tilde{u}_{x,l} = \langle u, \psi_{x,l} \rangle \tag{22}$$

with $\psi_{x,l}(y) = \frac{1}{l}[\delta(\frac{y-x}{l}+1) - \delta(\frac{y-x}{l})]$. Note that the wavelet is normalized with respect to the L^1-norm. The p-th order structure function $S_p(l)$ therefore corresponds to the p-th order moment of the wavelet coefficients at scale l,

$$S_p(l) = \int |\tilde{u}_{x,l}|^p dx. \tag{23}$$

As the DOD wavelet has only one vanishing moment (its mean), the exponent of the p-th order structure function in the case of a self-similar behaviour is limited by p, *i.e.* if $S_p(l) \propto l^{\zeta(p)}$ then $\zeta(p) < p$. This 'saturation' behaviour was originally observed by Babiano et al. [1] for DNS of two-dimensional flows. To be able to detect larger exponents one has to use increments with a larger stencil, or wavelets with

more vanishing moments, *i.e.* $\int x^m \psi(x) dx = 0$ for $m = 0, 1, \ldots, M-1$. This will become clearer below in the context of Besov regularity of functions.

We now concentrate on the case $p = 2$, *i.e.* the energy norm. Equation (16) gives the relation between the global wavelet spectrum $\widetilde{E}(k)$ and the Fourier spectrum $E(k)$ for an arbitrary wavelet ψ. For the DOD wavelet we find, since $\hat{\psi}(k) = e^{ik} - 1 = e^{ik/2}(e^{ik/2} - e^{ik/2})$ and hence $|\hat{\psi}(k)|^2 = 2(1 - \cos k)$, that

$$\widetilde{E}(k) = \frac{2}{C_\psi k} \int_0^\infty E(k')(1 - \cos(\frac{k_0 k'}{k}))\, dk'. \tag{24}$$

Setting $l = k_0/k$ and comparing with (10) we see that the wavelet spectrum corresponds to the second order structure function, *i.e.*

$$\widetilde{E}(k) = \frac{1}{C_\psi k}\, S_2(l). \tag{25}$$

The above results show that, if the Fourier spectrum behaves like $k^{-\alpha}$ (for $k \to \infty$), $\widetilde{E}(k) \propto k^{-\alpha}$ if $\alpha < 2m + 1$, where m is the number of vanishing moments of the wavelets. Consequently we find for $S_2(l)$ that $S_2(l) \propto l^{\zeta(p)} = \left(\frac{k_0}{k}\right)^{\zeta(p)}$ (for $l \to 0$) if $\zeta(2) \leq 2M$. In the present case we have $M = 1$, *i.e.* the second order structure function can only detect slopes smaller than 2, corresponding to an energy spectrum with slopes shallower than -3. Thus we find that the usual structure function gives spurious results for sufficiently smooth signals. In the appendix we generalize the relation between structure functions and wavelet coefficients by introducing Besov spaces which are typically used in nonlinear approximation theory [7].

4 Application to two-dimensional turbulence

4.1 Classical statistical analysis

We now analyze quantitatively the emergence of intermittency in a two-dimensional homogeneous isotropic decaying flow. The two-dimensional Navier–Stokes equations

$$\partial_t \omega + \vec{u} \cdot \nabla \omega = \frac{1}{Re} \nabla^2 \omega \tag{26}$$

where $\vec{u}$ is the velocity, $\omega = \nabla \times \vec{u}$ is the vorticity, and Re is the Reynolds number (based on the size of the domain), are computed for periodic boundary conditions using a pseudo-spectral direct numerical simulation at resolution 256^2. The Navier–Stokes dynamics rapidly organize the initial homogeneous flow into isolated coherent vortices which contain most of the vorticity, and this process results in an intermittent distribution of vorticity (figure 1). The idea that intermittency arises from instabilities which generate coherent vortices was already inferred by Batchelor & Townsend [2] from experimental data, when they wrote:

> It is suggested that the spatial inhomogeneity is produced early in the history of the turbulence by an intrinsic instability, in the way that a vortex sheet quickly rolls up into a number of strong discrete vortices.

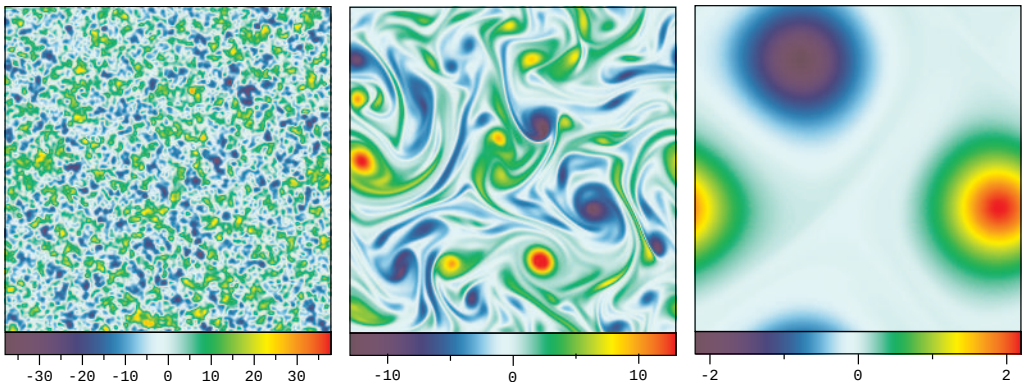

Figure 1. Vorticity field at $t = 0, 4, 100$. Note the emergence of coherent vortices from an initially homogeneous vorticity distribution.

Note that in our case the initial vorticity field, although homogeneous, contains extreme values associated with the tails of the Gaussian PDF (cf. figure 2) which act as seeds for the formation of coherent vortices.

We now analyze quantitatively the emergence of intermittency in a homogeneous two-dimensional turbulent flow at Reynolds number $Re = 1\,000$. This evolution may be divided into three different stages:

- At early times, from $t = 0$ to $t = 4$, the vorticity dynamics are dominated by strong dissipation of enstrophy $Z = 1/2 \int |\omega|^2 dx$ and palinstrophy $P = 1/2 \int |\nabla\omega|^2 dx$: 89% of the initial enstrophy Z_0 and 98% of the initial palinstrophy P_0 are dissipated between $t = 0$ to $t = 4$ (cf. table 1). This stage corresponds to the formation of coherent vortices which emerge from the random initial vorticity distribution.

- At intermediate times, from $t = 4$ to $t = 10$, both enstrophy and palinstrophy decay more slowly: $60\%Z_0$ and $88\%P_0$ are dissipated between $t = 4$ and $t = 10$ (cf. table 1). During this stage the flow dynamics is dominated by strong nonlinear vortex interactions.

- At later times, from $t = 10$ to $t = 100$, the energy decreases very slowly (cf. table 1), and the flow evolves towards a quasi-stationary state where only two opposite-sign coherent vortices remain.

After the last stage the turbulence is effectively dead, as the nonlinear dynamics are zero (*i.e.* $\vec{u} \cdot \nabla\omega \approx 0$), and the flow evolves exclusively due to the diffusion of vorticity.

We now analyze these three stages in more detail using the measures introduced earlier. The random initial distribution of vorticity (figure 1 a) is characterized by a Gaussian PDF (figure 2 a) and a large scale correlation (figure 4 a). At early times (from $t = 0$ to $t = 4$) the Navier–Stokes nonlinear dynamics leads to a self-

organization of the vorticity field into isolated coherent vortices (figure 1 b). The formation of coherent vortices is reflected in the following quantities:

- Vorticity in physical space changes from homogeneous at $t = 0$ (figure 1a) to inhomogeneous (figure 1b) at later times.
- The PDF of vorticity changes from a Gaussian at $t = 0$ (figure 2a) to a stretched exponential (figure 2b) at later times.
- The scatter-plot of ω versus Ψ changes from decorrelated at $t = 0$ (figure 3a) to correlated as a superposition of several functional relationships $\omega = F(\Psi)$ (figure 3b), each corresponding to a coherent vortex.
- Wavelet coefficients of vorticity $\tilde{\omega}$ change from dense for the Gaussian distribution at $t = 0$ (not shown here) to sparse (figure 5d) at later times.

At the intermediate and late stages for $t = 4$ to $t = 100$ the flow dynamics is dominated by the nonlinear interactions between isolated coherent vortices. Each vortex is advected and strained by the velocity resulting from all vortex motions; this evolution is conservative (without dissipation) as long as the vortices are far apart. If two vortices of the same sign move close together the interaction is no longer conservative and leads to the fusion of the vortices accompanied by a strong (although very intermittent in space and time) dissipation of enstrophy and palinstrophy. By $t = 100$ the flow has reached a quasi-stationary state where all same-sign vortices have merged and only two opposite-sign vortices remain. This final stage is characterized by two distributions predicted by analytical theories, as we will now explain.

As shown in figure 2, the initial Gaussian distribution evolves via a stretched exponential to a quasi-stationary final state approximating a Cauchy distribution. This Cauchy distribution agrees with the prediction of Min, Mezić & Leonard [24] based on a system of point vortices. For such a distribution the variance and all higher order moments diverge, showing that the Navier–Stokes equations can generate extremely non-Gaussian distributions with coherent vortices. This evolution of the PDF from Gaussian to Cauchy can be dynamically explained. Due to Biot–Savart's law the flow organizes itself around initial extreme values of the vorticity. The gradients formed between the coherent vortices by this process tend to dissipate weak vorticity and therefore isolate the vortices. The coherent vortices then merge, which results in further dissipation of weaker vorticity. As a result, the strong values of the vorticity decay more slowly than the weak values, which results in a steepening of the PDF. Note that the velocity remains quasi–Gaussian for all times, as is the case for three-dimensional turbulence.

The coherence scatter plot (pointwise correlation between vorticity and stream function) illustrates the self-organization of the flow (see figure 3). Initially there is no correlation between the stream function Ψ and the vorticity ω, while in the final state a functional relation $\omega = F(\Psi)$, with $F(\Psi) = \alpha \sinh(|\beta|\Psi)$ where $\alpha = 1/5$ and $\beta = -2$, emerges. The functional relationship between ω and Ψ implies that the nonlinearity has been depleted, and that the flow has reached a quasi-stationary state. This sinh functional relationship was predicted by Joyce & Montgomery [15]

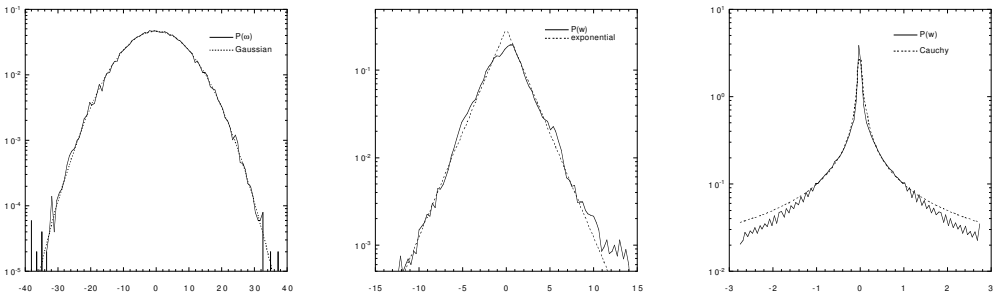

Figure 2. PDF of vorticity field at $t = 0, 4, 100$. The PDF is initially Gaussian and changes to a Cauchy distribution via a stretched exponential. The dotted curves show the ideal distribution (Gaussian, stretched exponential or Cauchy).

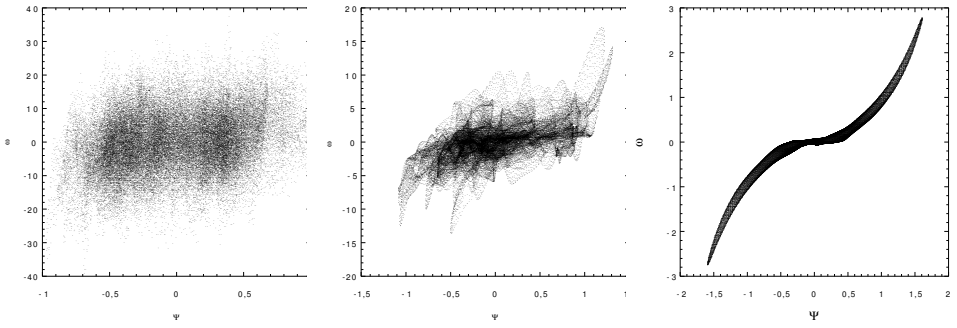

Figure 3. Coherence scatter plot at $t = 0, 4, 100$. Note the transition from an uncorrelated state towards a functional relationship $\omega = F(\Psi)$, characteristic of quasi-stationary coherent vortices.

and verified numerically by Montgomery *et al.* [25]. At intermediate times the coherence scatter plot appears to be a superposition of many sinh curves with different α and β corresponding to the many individual coherent vortices (the thickening of the curves is due to the relative motion of the vortices). The coherence plot measures the organization of the flow, and shows that as the flow becomes more organized the statistics become less Gaussian. We consider the conjunction of these two effects to be characteristic for intermittency in incompressible turbulent flows.

In figure 4(a), we show the time evolution of the energy spectrum at $t = 0, 4$ and 100. It follows a power law in the inertial range, namely from $k = 1$ up to the dissipative wavenumbers larger than $k = 64$, where the slope changes from -3 at $t = 0$, to -4 at $t = 4$ and finally to -6 at $t = 100$. These negative slopes reveal the long range correlation of the energy spectrum which increases in time, *i.e.* the velocity field becomes increasingly correlated and smooth. Note that the statistical theory of two–dimensional homogeneous turbulence [19] predicts a k^{-3} power-law

Table 1. Statistics of the decaying turbulence simulation, where E denotes the energy, Z the enstrophy, P the palinstrophy and M_p the p-th oder moments of vorticity.

t	E	Z	P	$M_3/M_2^{3/2}$	M_4/M_2^2	$M_5/M_2^{5/2}$	M_6/M_2^3
0	0.5000	37.38	28312.6	-0.01028	3.061	-0.1926	15.83
4	0.3949	4.146	529.2	0.3436	5.676	8.325	76.36
10	0.3453	1.739	61.97	0.8891	8.147	21.81	150.4
100	0.2546	0.3076	0.5831	0.04206	5.766	0.4563	46.23

behaviour. The steepening of the slope we observe as time evolves is attributed to the intermittency resulting from the emergence of coherent vortices [22].

In table 1, we show the time evolution of the ratio between the subsequent moments of vorticity $M_p/M_2^{p/2}$. At time $t = 0$ the behaviour of $M_p/M_2^{p/2}$ versus p is consistent with the Gaussianity of the initial vorticity distribution. At later times, the ratio increases with p faster than for the Gaussian distribution, which confirms the fact that the vorticity field becomes intermittent, as we have already seen from the vorticity (cf. figure 2)

4.2 Wavelet statistical analysis

We now apply the wavelet diagnostics introduced in §3 to analyze the intermittency of the freely decaying two-dimensional turbulent flow described in the previous section.

In figure 4 (b) we show the scale dependence of enstrophy (15) at early, intermediate and late times. The scale l of maximum enstrophy increases from $l = 2^{-5}$ at $t = 0$ to $l = 2^{-2}$ at $t = 100$. Therefore this correlation scale of the vorticity field increases in time, which is due to the formation and subsequent merging of coherent vortices, as illustrated in figure 1.

The scale dependent flatness of vorticity F_j is shown in figure 4(c). It evolves from Gaussian (*i.e.* $F_j \approx 3$ for all j) at $t = 0$ to non-Gaussian (characterized by the fact that F_j strongly increases with scale j) as time increases.

We focus now on the instant $t = 4$ (cf. figure 1b), which is typical of the regime where coherent vortices have already formed and are interacting strongly. To study the dynamics of this flow regime we analyze the vorticity field ω, the linear dissipation term $L = 1/Re\,\nabla^2\omega$ and the nonlinear advection term $N = -\vec{u}\cdot\nabla\omega$ of the governing vorticity transport equation

$$\partial_t\omega = L + N \tag{27}$$

at time $t = 4$. We recall that, since $\nabla\cdot\vec{u} = 0$, the velocity can be reconstructed from the vorticity using Biot–Savart's relation, $\vec{u} = \nabla^\perp\nabla^{-2}\omega$, where $\nabla^\perp = (-\partial_y, \partial_x)$ and ∇^{-2} denotes the Green's function of the Laplacian. We plot vorticity, dissipation and advection at $t = 4$ in both physical and wavelet space in figure 5. Figure 5b shows that dissipation is localized in the sheared regions between interacting vortices. Figure 5c) shows that the advection term is also well-localized in sheet-like regions. The wavelet coefficients of the three fields have similar intermittent

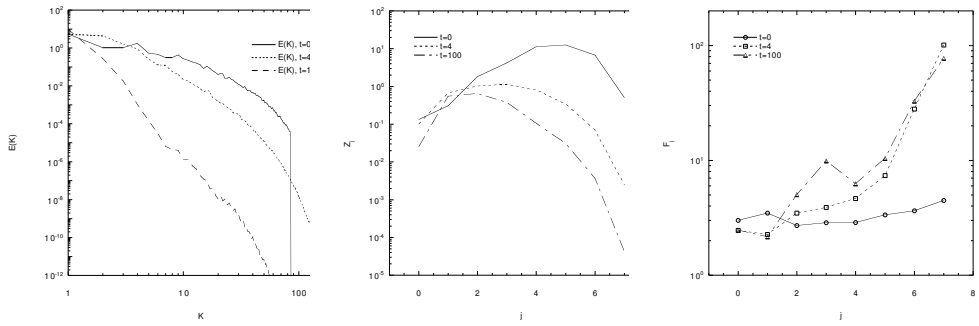

Figure 4. (a) Energy spectra $E(k)$. (b) Scale distribution of enstrophy Z_j. (c) Scale dependent flatness F_j at $t = 0, 4, 100$ for the decaying case.

structure. Note that the wavelet coefficients become increasingly sparse at smaller scales (figure 5d, e, f), which is a good indication of intermittency. It is interesting to note that the wavelet coefficients that are active for vorticity are also active for dissipation and advection, *i.e.* the same wavelet coefficients represent all three quantities.

The wavelet coefficients $\tilde{\omega}$, $\tilde{L}$ and $\tilde{N}$ reveal that vorticity, dissipation and advection are strongly intermittent, *i.e.* for these 3 fields the spatial support decreases with the scale, likewise their wavelet coefficients become sparser when scale decreases. This intermittency is quantified by computing the scale dependent flatness F_j (c.f. figure 6c). The moments M_p and the flatness F_j strongly increase with p and j, respectively, with the same scaling law for the three fields ω, L and N. This confirms the fact that they have the same type of intermittency.

In figure 6a we display the scale distribution (in L^2-norm) of vorticity, dissipation and advection. They all are multiscale, but have different distributions: vorticity is most active around scale $l = 2^{-2.5}$, dissipation around scale $l = 2^{-6}$ and advection around scale $l = 2^{-5}$. The fact that dissipation has its maximum at small scales agrees with the classical phenomenology. However, its multiscale distribution contradicts the assumption of a non-dissipative inertial range (assumed by the statistical theory of turbulence), but agrees with the hypothesis of progressive dissipation throughout the inertial range as proposed by Castaing [5], and Frisch & Vergassola [13], for three-dimensional turbulence.

Now we take the vorticity field at $t = 4$ and randomize the phase of its Fourier coefficients, in order to construct a fractal field with a Gaussian PDF, retaining the spatial correlation of the original vorticity field. The randomized vorticity field ω_r is defined as

$$\omega_r(\vec{x}) = \sum_{\vec{k}} |\widehat{\omega}(\vec{k})|\, e^{i\theta} e^{i\vec{k}\cdot\vec{x}}, \tag{28}$$

where $\widehat{\omega}(\vec{k}) = 1/(2\pi) \int \omega(\vec{x}) \exp(-i\vec{k}\cdot\vec{x}) d\vec{x}$ denotes the Fourier transform of the original vorticity field and θ are uniformly distributed random numbers, *i.e.*

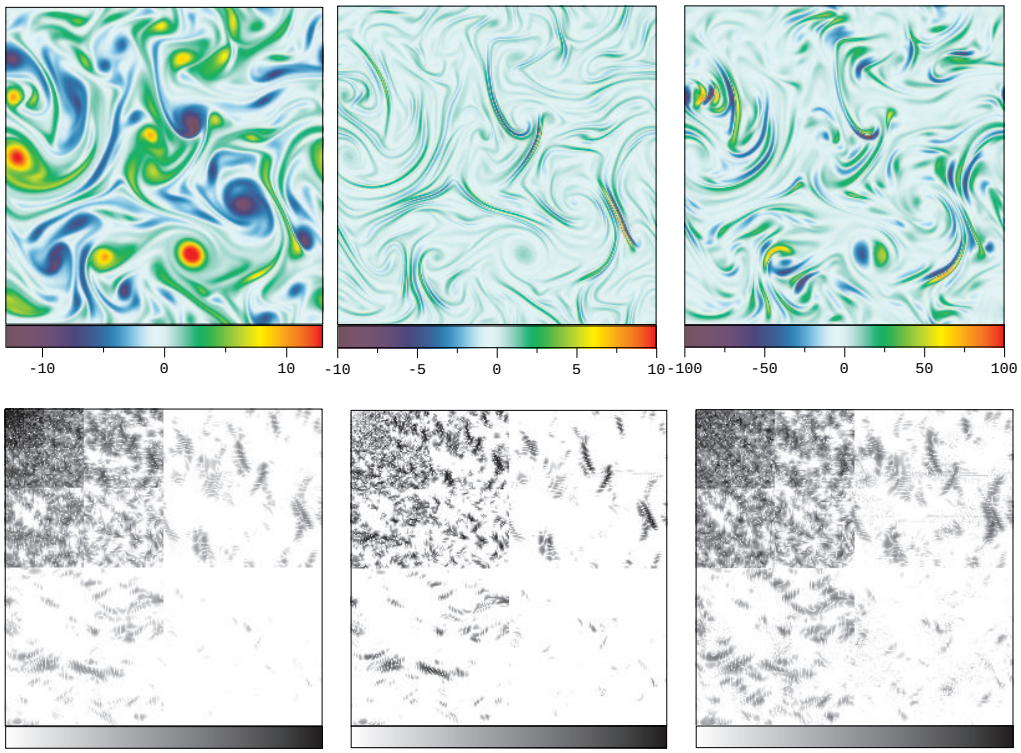

Figure 5. Top: vorticity field ω, linear dissipation term $L = -1/Re\,\nabla^2\omega$ and nonlinear advection term $N = \vec{u}\cdot\nabla\omega$ at $t = 4$. Bottom: the corresponding wavelet coefficients $\tilde{\omega}$, $\tilde{L}$ and $\tilde{N}$. We use the Mallat representation [21] for the wavelet coefficients.

$\theta \in U(0,1)$. Although the resulting field has the same spectral behaviour (cf. figure 7b) and the same scale distribution (cf. figure 7c) as vorticity ω, it has neither coherent vortices in physical space (figure 7a), nor intermittency, *i.e.* its wavelet coefficients are not sparse at small scales (figure 7d). The phase-scrambled field also has no significant increase of flatness F_j with scale (figure 7f). Its PDF is Gaussian with flatness $F = 2.9$ (cf. figure 7e), compared with $F = 5.7$ and stretched exponential PDF for the original field (figure 2b). We have thus shown that a fractal field with the same long-range dependence as a turbulent field (*i.e.* same energy spectrum) is not necessarily intermittent. This also demonstrates that intermittency in turbulence is due the presence of coherent vortices.

To illustrate the relation between structure functions and scale dependent moments of the wavelet coefficients we consider a typical statistically stationary two-dimensional turbulent flow field at resolution $N = 256^2$, extensively studied in [10]. In fig. 8 (top, left) we plotted its energy and enstrophy spectra exhibiting a k^{-5} and a k^{-3} power law behaviour, respectively. Figure 8 (top, right) shows the enstrophy Fourier spectrum together with the global wavelet spectrum using quintic spline

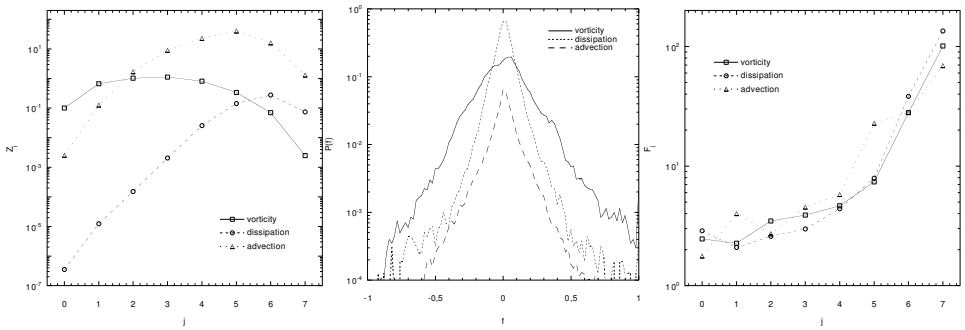

Figure 6. Scale distribution of enstrophy Z_j, normalized PDFs $P(f_n)$ for $f_n = f/||f||_\infty$ and scale-dependent flatness F_j for vorticity, dissipation and advection terms at $t = 4$.

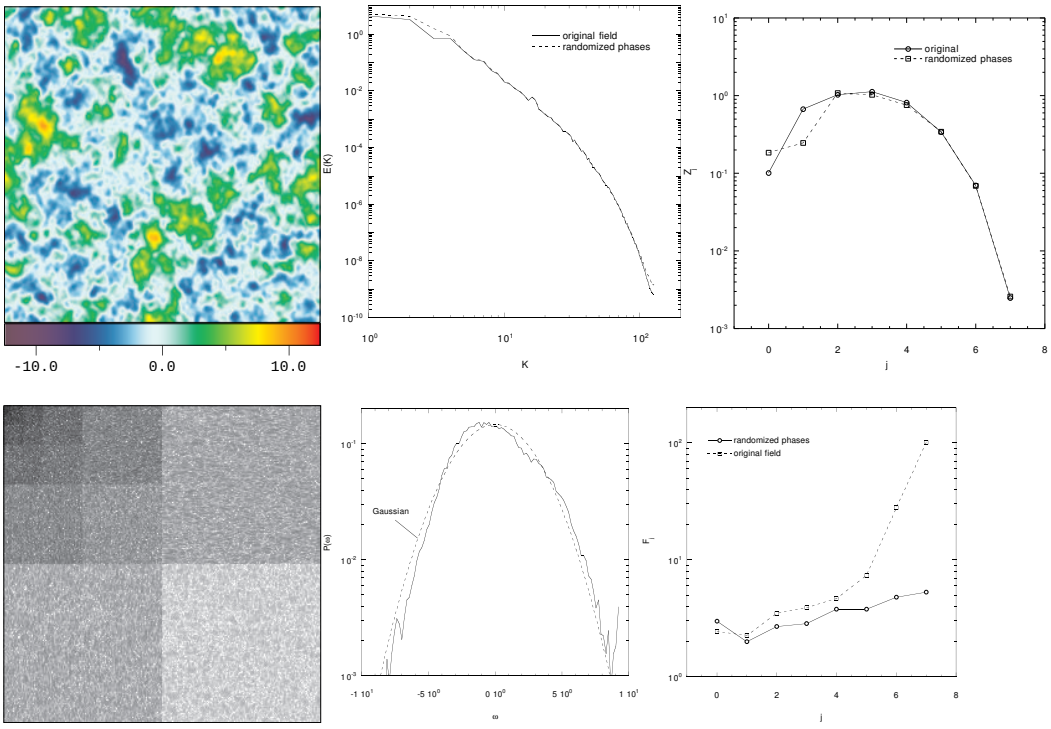

Figure 7. Top: vorticity with randomized phases, ω_r at $t = 4$. Corresponding energy spectra $E(k)$ and scale distribution of enstrophy Z_j. Bottom: corresponding wavelet coefficients $\tilde{\omega}_r$, PDF of vorticity ω_r and flatness F_j.

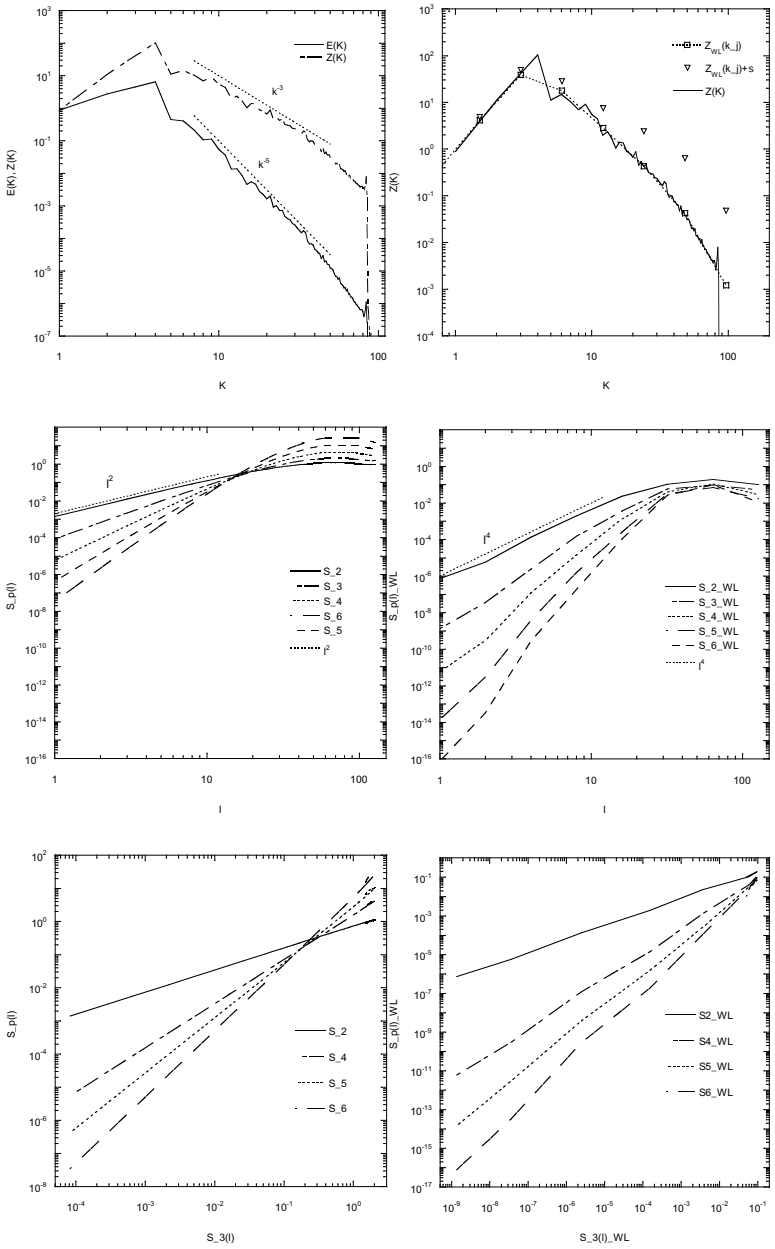

Figure 8. Top: Isotropic Fourier energy and enstrophy spectra (left). Fourier and global wavelet enstrophy spectra and the standard deviation of the wavelet spectrum in physical space. Middle: Classical longitudinal structure functions $S_{||,p}(l)$ for $p = 2, ..., 6$ of velocity (left) and corresponding wavelet based longitudinal structure functions (right), both averaged over 256 lines. Bottom: Structure functions versus third order structure function, left classical case, right wavelet case.

wavelets. We find perfect agreement between both Fourier and wavelet spectra as predicted by the theory (16) since the wavelet used here has 5 vanishing moments. Furthermore we plot the global wavelet spectrum, plus its standard deviation at different scales, to illustrate the fact that the fluctuations of the spectrum in physical space increase with the wavenumber. All these diagnostics indicate the presence of intermittency.

In figure 8 (middle) we plot the longitudinal structure functions $S_{||,p}(l)$ of the velocity for $p = 1$ to 6. On figure 8 (middle, left) we use the DOD wavelet, *i.e.* the classical structure function, and on figure 8 (middle, right) we use quintic spline wavelets. For the classical structure functions (figure 8 (middle, left)) we observe that the slope is limited by the number of vanishing moments of the wavelet. For example at $p = 2$ we observe that $S_2(l) \propto l^2$, whereas one should find for $S_2(l) \propto l^4$ since $E(k) \propto k^{-5}$. This limitation is due to the fact that the DOD wavelet has vanishing mean only, and therefore the structure functions show the scaling of the wavelet ($\zeta(p) = p$) and not that of the velocity field! Using the quintic spline wavelets instead of the DOD wavelets, we find the correct slope of l^4 for S_2, since the quintic spline wavelets have 5 vanishing moments. For the higher order structure functions we find $\zeta(p) \approx 2p$, which is the expected scaling of a two-dimensional velocity field.

4.3 Extended self-similarity

To extend the scaling behaviour of structure functions one typically uses rescaled structure functions [3], *i.e.* one considers ratios of structure functions of different order $S_p(l)/S_q(l)$. One then studies the scaling behaviour of the p-th order structure function as a function of the q-th order structure function, *i.e.*

$$S_p(l) \propto S_q(l)^{\zeta(p,q)} \tag{29}$$

with $S_q(l) \propto l^{\zeta(q)}$. Typically, $q = 3$ due to the fact that $S_3(l)$ is known exactly from the Karman–Howarth equation [14]. This approach is called extended self-similarity (ESS). It greatly increases the range over which one observes a well-defined power-law, even at moderate Reynolds numbers.

Because the scale-dependent moments of the wavelet coefficients are equivalent to the structure functions using the L^1 normalization of the wavelets, *i.e.* $S_p^{WL}(2^{-j}) = 2^{jp/2} M_{p,j}(f) = 2^{jp/2}/2^j \sum_{i=0}^{2^j-1} |\tilde{f}_{j,i}|^p$, the ratios of the moments at different scales $Q_{p,q,j}(f)$ (20) correspond to a generalized extended self similarity in wavelet space. This allows us to detect the self-similar behaviour of functions with steeper slopes: if ψ has m vanishing moments then $\zeta(p)$ is bounded from above by mp.

Finally, in figure 8 (bottom) we plot the structure functions versus the third order structure function, as used in the ESS approach. In both cases we observe that the functions are less curved than without using ESS. For the classical structure functions based on the DOD wavelet (figure 8 bottom, left), we find slopes of $2/3, 4/3, 5/3$ and 2 for $p = 2, 4, 5$ and 6, respectively. When we use the improved structure function based on the quintic spline wavelet, we find the same slopes of $2/3, 4/3, 5/3$ and 2 for $p = 2, 4, 5$ and 6, respectively. This is due to the fact the

we plot the structure functions versus the third order structure function and hence only information about the relative slope is obtained.

The above results show that the slope of the classical structure functions is limited by the regularity of the underlying DOD wavelet. The scaling behaviour of smoother fields can only be detected using structure functions based on wavelets with a sufficient number of vanishing moments. We have also shown that the ESS approach may be misleading, as it only yields information about the relative slopes. These relative slopes might be the same, even if the slopes of the original structure functions are wrong.

The relations summarized in this section have been presented for the one-dimensional case only, but they can be generalized easily to higher dimensions using tensor product constructions of wavelets [6] and Besov spaces in $\mathbb{R}^n$ [32].

5 Conclusion

In this paper we have reviewed the usual ways of quantifying turbulence intermittency and its effects. In particular, we have emphasised the fact that structure functions can be interpreted as wavelet transformed quantities using a difference of Diracs (DOD) wavelet. Because this wavelet is singular, it is insensitive to sufficiently smooth signals. This means that for signals with an energy spectrum steeper than -3 the classical structure function gives spurious results. In order to overcome this limitation we propose using a sufficiently smooth wavelet (*i.e.* one with more zero moments). This point has been illustrated using the velocity field from a two-dimensional DNS which has an energy spectrum with a slope -5. We have found that the classical structure functions merely measure the properties of the DOD wavelet, whereas the structure functions based on a smoother (quintic spline) wavelet provide accurate scalings.

We have also presented several other wavelet-based diagnostics to quantify intermittency. Each of them exploits the space–scale localization properties of the wavelet representation, that reflects the space–scale localization of intermittency itself. The characteristics of intermittent fields were highlighted by applying these wavelet tools to a decaying two-dimensional turbulence, and to a non-intermittent Gaussian random field with the same energy spectrum. These wavelet diagnostics also showed that the nonlinear advection term and the linear dissipation term of Navier–Stokes equations are highly intermittent. This justifies the use of adaptive wavelet-based algorithms [31], that exploit this intermittency to reduce the number of degrees of freedom necessary to compute the evolution of turbulent flows.

We have also studied the appearance of intermittency in a turbulent flow computed from non-intermittent initial conditions until it reaches a final quasi-stationary state. We showed how the nonlinear dynamics of the Navier–Stokes equations produces a highly intermittent vorticity distribution due to the formation of coherent vortices.

Finally, we would like to emphasize that the wavelet measures of intermittency presented here are not specific to turbulence, and therefore can be applied to other intermittent signals.

Acknowledgements
We gratefully acknowledge financial support from McMaster University, the programme pluri–formation 'Modélisation et simulation numérique en mécanique des fluides' of Ecole Normale Supérieure Paris, the European Program TMR on 'Wavelets in Numerical Simulation' (contract FMRX-CT 98–0184) and the French–German Program Procope (contract 99090). N. Kevlahan would like to thank NSERC and CNRS for financial support, and he would especially like to thank M. Farge for the chance to visit LMD during part of this work.

Appendix

The relation between structure functions and wavelet coefficients can be generalized by using appropriate function spaces. For this we introduce Besov spaces [32,7], which can be characterized using wavelet coefficients and are related to structure functions [27].

For $q < \infty$ we define the Besov space

$$\mathcal{B}^s_{p,q} = \left\{ f \in L^p(I\!R) \ ; \ l^{-s}\Big(\int |f(x+l) - f(x)|^p dx\Big)^{1/p} \in L^q(I\!R^*_+, \frac{dl}{l}) \right\} \tag{30}$$

with $0 < s < 1$, $p, q \geq 1$.

This means that $f \in \mathcal{B}^s_{p,q}$ if and only if $f \in L^p$, and

$$\left(\int_0^{+\infty} l^{-sq} \Big(\int |f(x+l) - f(x)|^p dx \Big)^{p/q} \ \frac{dl}{l} \right)^{\frac{1}{q}} < \infty \ . \tag{31}$$

Using the p-th order structure function $S_p(l)$, this is equivalent to

$$\left(\int_0^{+\infty} l^{-sq} \ S_p(l)^{\frac{q}{p}} \frac{dl}{l} \right)^{\frac{1}{q}} < \infty. \tag{32}$$

This means that the p-th order structure function is related to Besov norms via the modulus of continuity.

The corresponding norm is given by

$$||f||_{\mathcal{B}^s_{p,q}} = ||f||_{L^p} + |f|_{\mathcal{B}^s_{p,q}} \tag{33}$$

where the semi-norm $|f|_{\mathcal{B}^s_{p,q}}$ is defined as:

$$|f|_{\mathcal{B}^s_{p,q}} = \left(\int_0^{+\infty} \Big[l^{-s} \ \Big(\int |f(x+l) - f(x)|^p dx \Big)^{1/p} \Big]^q \ \frac{dl}{l} \right)^{\frac{1}{q}} \tag{34}$$

$$= \left(\int_0^{+\infty} l^{-sq} \ S_p(l)^{\frac{q}{p}} \ \frac{dl}{l} \right)^{\frac{1}{q}} \tag{35}$$

$$\approx \left(\int_0^{+\infty} \Big[a^{-\alpha} \ ||\widetilde{f}(a,\cdot)||_{L^p} \Big]^q \ \frac{da}{a} \right)^{\frac{1}{q}}. \tag{36}$$

This shows that the Besov norms ($q < \infty$) are intimately related to the structure functions $S_p(l)$ and the wavelet coefficients $\widetilde{f}(a,\cdot) = \langle f(x), \psi_{a,b}(x) \rangle$.

In the case $q = \infty$, we obtain

$$\mathcal{B}^s_{p,\infty} = \left\{ f \in L^p(I\!R) \ ; \ l^{-s}(\int |f(x+l) - f(x)|^p dx)^{1/p} \in L^\infty(I\!R^*_+) \right\} \tag{37}$$

and for the semi-norm we get

$$|f|_{\mathcal{B}^s_{p,\infty}} = ||l^{-s}(\int |f(x+l) - f(x)|^p dx)^{1/p}||_\infty = ||l^{-s} S_p(l)^{1/p}||_\infty. \tag{38}$$

In the case of a self-similar behaviour of the type

$$S_p(l) \sim l^{\xi(p)} \tag{39}$$

it follows that

$$f \in \mathcal{B}^{\xi(p)/p}_{p,\infty}. \tag{40}$$

This implies that $\xi(p) < p$ as we restricted ourself to the case $s < 1$. To overcome this limitation the Besov spaces can be generalized for $s > 1$, where s is no longer an integer. For $s > 1$, s not an integer, we decompose s into $s = [s] + \sigma$, ($[s]$ being the integer part of s) and we introduce

$$\mathcal{B}^s_{p,q}(I\!R) = \left\{ f \in L^p(I\!R) \ ; \ f^{(m)} \in \mathcal{B}^\sigma_{p,q}(I\!R) \, , \, 0 \le m \le [s] \right\} \tag{41}$$

where $f^{(m)}$ denotes the m-th derivative of f. The corresponding norm is defined as

$$||f||_{\mathcal{B}^s_{p,q}} = \sum_{m=0}^{[s]} ||f^{(m)}||_{\mathcal{B}^\sigma_{p,q}}. \tag{42}$$

In order to have norm equivalence with the wavelet coefficients, the wavelet ψ has to have at least $[s] + 1$ vanishing moments.

Let us mention that in the case where s is an integer, the modulus of continuity should be modified [32] to $||f(x+l) - 2f(x) - f(x-l)||_{L^p}$. Note that this second-order stencil is no longer equivalent to the structure function. Finally, when $p = q = 2$ we obtain the Sobolev space H^s and for $p = q = \infty$ the Hölder space C^s [32].

To summarize, structure functions of order p correspond to Besov norms of functions which can be characterized by means of weighted sums of wavelet coefficients due to norm equivalences. This remark completes the link between structure functions, wavelet coefficients and Besov norms. It also suggests that the limitations of classical structure functions may be overcome by using structure functions based on wavelets with more vanishing moments than the DOD wavelet.

References

1. Babiano, B., Basdevant, C. & Sadourny, R. 1985 Structure functions and dispersion laws in two–dimensional turbulence. *J. Atm. Sci.***42**(9), 941–949.
2. Batchelor, G. K. & Townsend, A. A. 1949 The nature of turbulent motion at large wave-number. *Proc. Roy. Soc.* A **199**, 238–255.
3. Benzi, R., Ciliberto, S., Tripicione, R., Baudet, C. & Massaioli, F. 1993 Extended self similarity in turbulent flows. *Phys. Rev. E* **48**, R29.

4. Chainais, P., Abry, P. & Pinton, J. 1999 Intermittency and coherent structures in a swirling flow: A wavelet analysis of joint pressure and velocity measurements. *Phys. Fluids* **11**(11), 3524–3539.
5. Castaing, B. 1989 Consequence d'un principe d'extremum en turbulence. *J. Physique* **59**, 147–156.
6. Daubechies, I. 1992 *Ten lectures on wavelets.* SIAM.
7. DeVore, R. 1999 Nonlinear approximation. *Acta Numerica* **8**, Cambridge University Press.
8. Do-Khac M., Basdevant C., Perrier V. and Dang-Tran K. 1990 Wavelet analysis of 2d turbulent flows. *Physica D*, **76**, 252–277.
9. Farge M., Pellegrino G. and Schneider K. 2001 Coherent Vortex Extraction in 3D Turbulent Flows using orthogonal wavelets. *Phys. Rev. Lett.*, **87**(5), 054501-1–054501-4.
10. Farge M., Schneider K. and Kevlahan N. 1999 Non–Gaussianity and Coherent Vortex Simulation for two–dimensional turbulence using an adaptive orthonormal wavelet basis. *Phys. Fluids*, **11**(8), 2187–2201. 117–200.
11. Farge, M. 1992 Wavelet transforms and their applications to turbulence. *Ann. Rev. Fluid Mech.* **24**, 395–457.
12. Farge, M. & Rabreau, G. 1988 Transformée en ondelettes pour détecter et analyser les structures cohérentes dans les écoulements turbulents bidimensionnels. *C. R. Acad. Sci. Paris Ser. II* **307**, 433–462.
13. Frisch, U. & Vergassola, M. 1991 A prediction of the multifractal model: the intermediate dissipation range. *Europhys. Lett.* **14**, 439–444.
14. Frisch, U. 1995 Turbulence. The legacy of A.N. Kolmogorov. Cambridge University Press.
15. Joyce, G. & Montgomery, D. 1973 Negative temperature states for the two-dimensional guiding-center plasma. *J. Plasma Phys.* **10**, 107.
16. Kennedy, D. A. & Corrsin, S. 1961 Spectral flatness factor and 'intermittency' in turbulence and in non-linear noise. *J. Fluid Mech.* **10**, 366–370.
17. Kolmogorov, A. N. 1941 The local structure of turbulence in incompressible fluid for very large Reynolds numbers. *Dokl. Akad. Nauk SSSR.* **30**(4), 301–305.
18. Kolmogorov, A. N. 1962 A refinement of previous hypotheses concerning the local structure of turbulence in a viscous incompressible fluid at high Reynolds number. *J. Fluid Mech.* **13**, 82–85.
19. Kraichnan, R.H. 1967 Inertial ranges in two-dimensional turbulence. *Phys. Fluids* **10**, 1417–1423.
20. Lin, C. C. 1953 On Taylor's hypothesis and the acceleration terms in the Navier-Stokes equations. *Quart. Appl. Math.* **10**(4), 295–306.
21. Mallat, S. 1998 A wavelet tour of signal processing. Academic Press.
22. McWilliams, J.C. 1984 The emergence of isolated coherent vortices in turbulent flows. *J. Fluid Mech.* ,**146**, 21–43.
23. Meneveau, C. 1991 Analysis of turbulence in the orthonormal wavelet representation. *J. Fluid Mech.* ,**232**, 469–520.
24. Min, I. A., Mezić, I. & Leonard, A. 1996 Lévy stable distributions for velocity and velocity difference in systems of vortex elements. *Phys. Fluids* **8**(5), 1169–

1180.
25. Montgomery, D., Matthaeus, W. H., Stribling, W. T., Martinez, D. & Oughton S. 1992 Relaxation in two dimensions and the "sinh-Poisson" equation. *Phys. Fluids* A, **4**, 3–6.
26. Obukhov, A. M. 1941 On the distribution of energy in the spectrum of turbulent flow. *Dokl. Akad. Nauk SSSR.* **32**(1), 22–24.
27. Perrier, V. & Basdevant, C. 1996 Besov norms in terms of the continuous wavelet transform. Applications to structure functions. *Math. Mod. Meth. Appl. Sci.* **6**, 649-664.
28. Perrier, V., Philipovitch, T. & Basdevant, C. 1995 Wavelet spectra compared to Fourier spectra. *J. Math. Phys.*, **36**(3), 1506–1519.
29. Sandborn, V. A. 1959 Measurements of intermittency of turbulent motion in a boundary layer. *J. Fluid Mech.* **6**, 221–240.
30. Schneider, K. & Farge, M. 1998 *Wavelet approach for modelling and computing turbulence.* In *Advances in turbulence modelling.* von Karman Institute for Fluid Dynamics Lecture Series 1998-05.
31. Schneider, K., Kevlahan, N. K.-R. & Farge, M. 1997 A comparison of an adaptive wavelet method and nonlinearly filtered pseudo-spectral methods for two-dimensional turbulence. *Theoret. Comput. Fluid Dynamics* **9**, 191.
32. Stein, E. M. 1970 *Singular integrals and differentiability properties of functions.* Princeton University Press.
33. Taylor, G. I. 1938 The spectrum of turbulence. *Proc. Roy. Soc. Lond.* A **164**, 476–490.
34. Townsend, A. A. 1948 Local isotropy in the turbulent wake of a cylinder. *Austr. J. Sci. Res.* **1**, 161.